Available online at www.sciencedirect.com

ScienceDirect

Ceramics International 40 (2014) 4461–4470

CERAMICS INTERNATIONAL

www.elsevier.com/locate/ceramint

Dense mullite zirconia composites obtained from the reaction sintering of milled stoichiometric alumina zircon mixtures by SPS

N.M. Rendtorff[a,b,*], G. Suárez[a,b,c], Y. Sakka[c], E.F. Aglietti[a,b]

[a]CETMIC, Centro de Tecnología de Recursos Minerales y Cerámica, Camino Centenario y 506, M.B.Gonnet, Buenos Aires, Argentina
[b]Dpto de Química, Facultad de Ciencias Exactas, Universidad Nacional de La Plata, 1 y 115 La Plata, CP 1900 Buenos Aires, Argentina
[c]Advanced Ceramic Group, Advanced Key Technologies Division, National Institute for Materials Science (NIMS), 1–2–1, Sengen, Tsukuba, Ibaraki 305–0047, Japan

Received 29 July 2013; received in revised form 28 August 2013; accepted 28 August 2013
Available online 12 September 2013

Abstract

The main objective of this article is to obtain dense (porosity under 0.5%) polyphasic ceramics belonging to the Al_2O_3–SiO_2–ZrO_2 system by SPS sintering of high energy powders milled drily; the stoichiometric (54.45:45.54 zircon–alumina, weight basis) mixture was explored in this work. Particularly the principal sintering variables: sintering temperature and dwell time were investigated. The textural, structural and microstructural changes were evaluated together with the hardness and toughness of the obtained ceramics and their microstructure. The effect of the mechanical pre-treatment was carried out by X-ray diffraction and particle distribution evaluation. Due to the rapid heating process an incomplete reaction was achieved in several cases, as a consequence multiphasic ceramics with different alumina, mullite, zircon and zirconia contents were obtained.

The mechanical pretreatment used resulted in a homogeneous dry mixture with a partial ($\approx$ 20%) zircon dissociation, apparently enhanced by the alumina presence. This together with the posterior SPS processing permitted to obtain fully dense ceramic composites at a very low temperature (1300 °C) without the requirement of any additive. The reactions from alumina zircon mixtures to mullite zirconia occur 200 °C below conventional processing routes and at least 50 °C below the reported SPS based materials processed from un-milled mixtures. The microstructure and mechanical properties obtained were comparable to the ones obtained by other processing routes. Finally some interesting group correlations were found for the developed materials while the hardness is directly correlated with the density and the fracture toughness is correlated with the zirconia (m+t) content.

Keywords: B. Composites; D. Mullite; Zirconia; Reaction sintering; SPS

1. Introduction

Ceramic materials from the Al_2O_3–SiO_2–ZrO_2 system are widely used in structural application in the steel and glass manufacturing industries, principally because of their high refractoriness, chemical resistance and adequate thermo-mechanical behavior [1,2]. The most used materials are those whose principal phases are alumina (Al_2O_3), mullite ($3Al_2O_3 \cdot 2SiO_2$), zircon ($ZrSiO_4$), and zirconia (ZrO_2) [1,2]. However, the same refractoriness makes the sintering of these materials difficult, hence sometimes different sintering additives are employed to fully dense these composites, but with some detriment in the properties and behaviors.

Particularly mullite–zirconia composites are materials with important technological applications due to their good properties such as toughness, chemical stability, and high-creep resistance. In practice they are employed in the glass industry and where high chemical and corrosion resistance are required. Zircon and alumina are largely employed as raw materials in their manufacture [1,2].

Unlike conventional methods like pressureless sintering and hot-pressing, Spark Plasma Sintering (SPS), a high density

*Corresponding author at: CETMIC, Centro de Tecnología de Recursos Minerales y Cerámica, Camino Centenario y 506, CC.49 B1897ZCA, M.B. Gonnet, Buenos Aires, Argentina.
Tel.: +54 221 4840247; fax: +54 221 4710075.
E-mail addresses: rendtorff@cetmic.unlp.edu.ar, rendtorff@hotmail.com (N.M. Rendtorff).

0272-8842/$ - see front matter © 2013 Elsevier Ltd and Techna Group S.r.l. All rights reserved.
http://dx.doi.org/10.1016/j.ceramint.2013.08.119

current activated sintering method, permits to reduce the sintering temperature and shorten the soaking time, resulting in a remarkable improvement on the properties of materials consolidated by this method. SPS resulted an efficient technique to obtain full density nanometric powders with negligible grain growth. A complete description of the technique can be found elsewhere [3–5].

The mechanochemical activation process has proved to be an effective technique to enhance a solid-state reaction at relatively low temperatures [6]. In these processes, the "mechanical" effects of milling, such as the reduction of particle size and mixture homogenization, are accompanied by chemical effects, such as partial loss of crystallinity resulting in very active reactants with high surface energy [6].

Recently this particular pre-treatment together with the SPS processing resulted to be suitable for obtaining adequate homogeneous mixtures of nanoscopic ceramic powders [7–10].

Much work has been carried out for obtaining mullite–zirconia composites by the reaction sintering of alumina–zircon mixtures [2] This reaction (Eq. (1)), typically takes place between 1400 °C and 1600 °C depending on the impurities and other phases. And is accompanied by sinterization, the accepted mechanisms implies the zircon dissociation in silica and zirconia followed by the mullite formation from silica and the alumina [2]. The effect of additives has been explored by different authors together with different processing routes [11–22].

$$2ZrSiO_4 + 3Al_2O_3 \rightarrow 2ZrO_2 + 3Al_2O_3 \cdot 2SiO_2 \quad (1)$$

Special attention must be taken into account for the differences in the thermal expansion of the different reagents and products of this solid state chemical reaction because an important mismatch will result. The actual values of the linear thermal expansion (between 30° and 1000 °C) are shown in Table 1. If the reaction is complete it can be easily observed that the expansion coefficient of zirconia (t–ZrO_2) is higher than mullite and the reagents, the differences are higher if the zirconia is tetragonal. This mismatch might result in the development of important internal stresses and its correspondent consequences during the sintering and subsequent thermal treatments [1,2].

Mullite–zirconia ceramic composites were also prepared by reaction sintering in spark plasma sintering (SPS) system. The starting material was plasma spheroidized (PS) zircon–alumina powders at 1000, 1100, 1200 and 1300 °C with duration of 10 and 30 min. At SPS temperature of 1000 °C, evidence of zircon decomposition is detected, while at 1200 °C, mullite formation dominates the process, resulting in significant increases in microhardness. Young's modulus and fracture toughness values [21], a combination of PS and SPS showed to be effective for preparing high performance mullite/ZrO_2 composites from zircon/alumina mixtures at a relatively low reaction sintering temperature. Recently pure Zircon and Zircon–Alumina ($ZrSiO_4$:α-Al_2O_3) (10% alumina) composite powders were subjected to densification studies employing spark plasma sintering (SPS) [23]. Physicochemical and microstructural properties of the samples were evaluated and compared with that of conventionally sintered compacts. Density measurements and microstructural evaluation revealed a low temperature densification of Zircon:Alumina at temperatures as low as 1300 °C by SPS. Increase of temperature to 1350 °C had shown negligible changes in density and on further heating the sample melts at 1400 °C as a result of excessive formation of liquid phase. However, pure zircon could not be densified in the absence of alumina under SPS conditions. It is evident that addition of alumina enhances partial low temperature decomposition of zircon under the influence of plasma generated during SPS.

Table 1
Mean Coefficient of linear expansion for the employed ceramic phases (30–1000 °C).

Material		Thermal expansion coefficient ($\times 10^{-6}$ °C^{-1})
Reagents	Zircon	4.2
	Alumina	8.8
Products	Mullite	5.3
	m–ZrO_2	6.5
	t–ZrO_2	10.0

On the other hand pure zircon was successfully densified by SPS with a high energy milling pretreatment, like the one applied in this work [9] zircon–zirconia composites were also densified by this method [10].

Finally it is important to point out that previously, Rocha-Rangel et. al. fabricated Mullite–ZrO_2 composites by attrition milling a powder mixture of zircon, alumina, and aluminum metal with MgO or TiO_2 as sintering additives, heating at 1100 °C to oxidize the aluminum metal, and consolidation by spark plasma sintering (SPS) [23]. The influence of the SPS temperature on different properties has been studied, including the mullite formation, the densification and the mechanical properties of the resulting composites. For the mullite–zirconia composites without sintering additives, the mullite formation was accomplished at 1540 °C, this temperature was lowered by the employed additives. Clay was employed as sintering additive for this kind of material with good results but with the disadvantage of incorporation of impurities [25].

The principal objective of this article is to obtain dense (porosity under 0.5%) polyphasic ceramics belonging to the Al_2O_3–SiO_2–ZrO_2 system by SPS sintering of drily high energy milled powders; the stoichiometric (54.45:45.54 zircon–alumina, weight basis) mixture was explored in this work. Particularly the principal sintering variables: sintering temperature and soaking time were investigated. The textural, structural and microstructural changes were evaluated together with the hardness and toughness of the obtained ceramics. The effect of the mechanical pre-treatment was carried out by X-ray diffraction and particle distribution evaluation. Due to the rapid heating process an incomplete reaction is expected, as a consequence multiphasic ceramics with different alumina, mullite, zircon and zirconia contents are expected. Having scaling up in mind the aim is to obtain composite material from commercial powders, not requiring the use of any

additive ceramic materials with adequate mechanical properties.

2. Experimental procedure

The zircon starting powder was zirconium silicate with ZrO_2 = 64–65.5 wt%, SiO_2 = 33–34 wt%, $Fe_2O_3 \leq 0.10$ wt% and $TiO_2 \leq 0.15$ wt%, mean diameter (D_{50}) of 2.0 μm, specific gravity of 4.6 g/cm^3, melting point of 2200 °C and hardness (Mohs) of 7.5 (Kreutzonit Super, Mahlwerke Kreutz, Germany). The second starting powder was Alumina (ALCOA A16-SG) α-alumina (d_{50} = 0.45 μm). (Al_2O_3: 99.7%, SiO_2: 0.025 wt%.)

An initial pre-mixture of powders (54.45:45.54 zircon-alumina, weight basis) mechanically mixed in ethanol (traditional ball mill for 2 h with alumina balls with 10 mm diameter). After drying, in order to enhance the SPS kinetics, the powder mixture with high surface activation was drily milled using a high energy planetary mill (7 Premium Line, Fritsch Co., Ltd., Germany). To minimize contamination during the HEBM the jar and milling media employed were of Zirconia; 85 ml jars were used with 60 g of balls (3 mm diameter) as milling media; the ratio between the weight of powder and the milling balls was 1:10 in each batch [24]. A 900 rpm rotation speed was used; in these conditions the milling is so energetic that the jars were left to cool down for 90 min every 5 min of HEBM the milling time employed was 60 min, based in the results obtained in a similar system.

Although the effect of the milling pre-treatment is not the principal aim of this work; this work is focused mainly on the posterior sintering of this powder, and the properties of the obtained ceramics. Nevertheless some characterization was carried out. This pretreatment has demonstrated recently the effectiveness for the posterior SPS sintering [10] being adequate to homogeneously mix two finely grained powders. As mentioned, the powder characterization comprised a SEM micrograph analysis (FEI Quanta 200), a particle size analysis and XRD-Rietveld analysis. The particle size analysis was carried out by laser scattering (Malvern Mastersizer 2000) in diluted (0.001 wt%) and ultrasonicated water dispersions.

Densification of the ball milled powders was conducted using an SPS machine (SPS–1050, Sumitomo, Kawasaki, Japan). Detailed information about the equipment and the sintering procedure can be found elsewhere [9]. The powder was placed into a graphite die with an inner diameter of 10 mm. In a typical sintering experiment, 1.0 g of milled powder was poured into the die. The temperature was measured accurately using a pyrometer focused on the die surface of the inner die (i.e., 1 cm far from the sample). Graphite felt was used to reduce the heat loss by radiation. The powder was heated from room temperature up to 700 °C for 10 min, subsequently, up to the sintering temperature (1100, 1200, 1300, 1400 and 1500 °C). The dwell time was 10 min and 100 MPa pressure was raised just after the beginning of the dwell time. In order to understand the reaction evolution, the 1400 °C treatment was studied for longer dwell times (between 10 and 60 min).

Density and apparent porosity of the sintered samples were evaluated by the Archimedes method. The crystalline phases of the ball-milled powders and of the SPSed specimens were determined by X-ray diffraction (XRD) using CuKα radiation operating at 40 kV and 300 mA, and quantified by the Rietveld Method [26,27]. The powders morphology and microstructure were made by scanning electron microscopy (SEM) (FEI Quanta 200, respectively). Vickers Hardness (Hv) and fracture toughness (K_{IC}) of the obtained ceramics were evaluated with a Vickers indentation machine (Buhueler, USA). At least six indents under 5 Kg load for each sample were performed. The fracture toughness (K_{IC}) was calculated by the following equation [9,28]:

$$K_{IC} = \delta\left(\frac{E}{Hv}\right)^{1/2}\frac{P}{c^{3/2}} \quad (2)$$

Where E is the elastic modulus, H is the Vickers Hardness, P is the indentation test load, c is the indentation crack length. Finally δ is a material-dependent constant that was assumed to be 0.018. The crack lengths were measured immediately after the indentation in order to avoid slow crack growth after removing the load. The E values employed were 240 GPa.

3. Results and discussions

3.1. Powders mechanical pretreatment

Fig. 1 shows the grain size (equivalent) distribution of the powders evaluated by laser scattering (Malvern Mastersizer 2000). The original alumina–zircon mixture (in red) corresponds to a peak and shoulder configuration which can easily deconvolute into two overlapped peaks which correspond to the grain size distribution of the as received alumina ($D_{50} \approx 0.45$ μm) and the zircon ($D_{50} \approx 2.0$ μm). On the other side, the resulting grain size distribution (plotted in green) corresponds to a straightforward bimodal (two peaks) distribution. With peaks centered at 0.5 μm and 4.0 μm. As a first glance, no important change in the grain distribution was observed. Some observations can be pointed out: while the first peak remains in the same center the second peak was moved to larger diameters. Moreover the first (alumina) is smaller than the corresponding one in the original powder, and the 4.0 μm

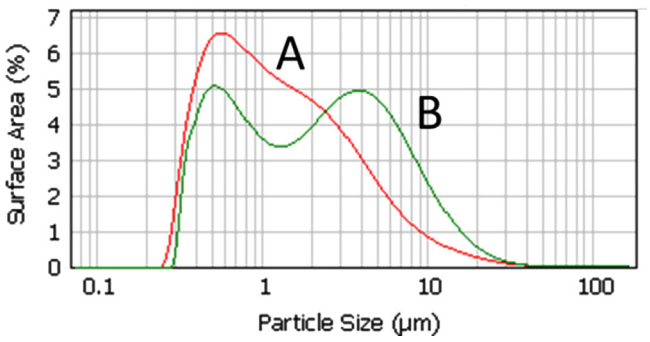

Fig. 1. Particle size distribution of the original mixture and the powder after the high energy milling treatment. (For interpretation of the references to color in this figure, the reader is referred to the web version of this article.)

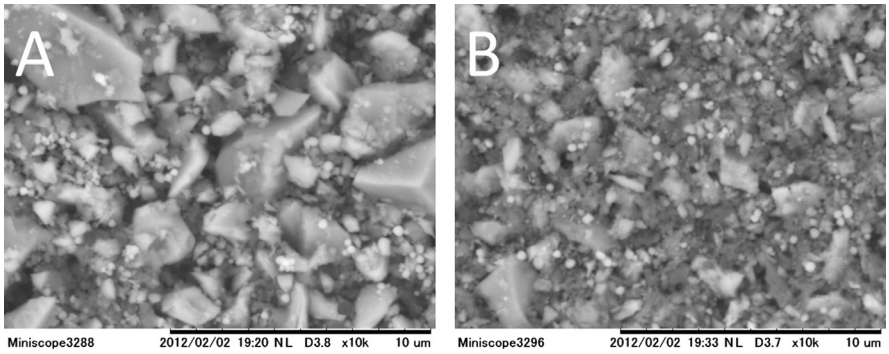

Fig. 2. SEM image of the powders before and after the high energy milling treatment (A and B respectively).

peak (zircon) is higher than the shoulder observed in the original powder. This could be explained by the fact that a fraction of the finer alumina grains covered the greater zircon grains increasing the apparent diameter of the zircon grains.

Fig. 2 A and B shows the SEM images of the original and milled alumina–zircon mixtures respectively. The bimodal distribution observed by scattering could be observed in both images with a noticeable morphology change in the greater zircon grains, which presented acute and angular shapes in the original powder and a more rounded morphology in the milled powder. The finer grains morphology could not be clearly observed.

In Fig. 3 the XRD patterns of the original and milled mixtures are shown. The pattern of the starting mixture, only shows alumina and zircon phases. The milled mixture presents the same peaks but with lower intensities showing that a loss in the crystallinity took place during the HEBM treatment. Furthermore tetragonal zirconia diffractions appeared. This was quantified, the zircon presented a partial ($\approx 20\%$) dissociation into zirconia and amorphous silica (undetectable by XRD) perhaps enhanced by the alumina presence. Alumina presence enhanced the thermal zircon dissociation in zirconia and silica [29]. This powder was directly employed as the only starting with no additive incorporated (Fig. 4).

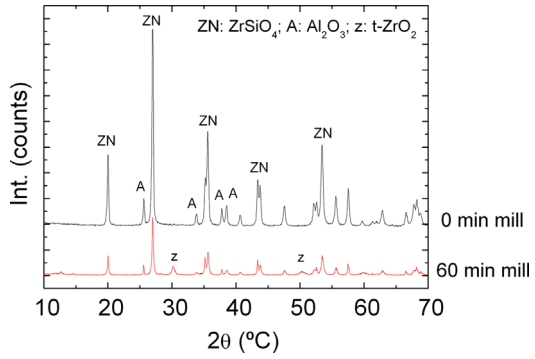

Fig. 3. XRD patterns of the original mixture and the powder after the high energy milling treatment.

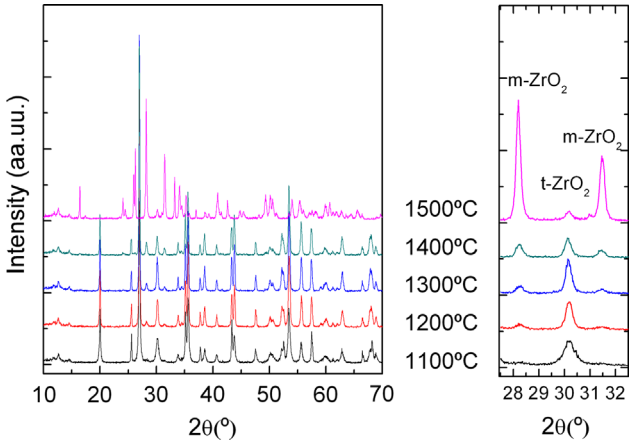

Fig. 4. XRD patterns of the ceramic composites sintered at different temperatures (10 min dwell).

3.2. SPS Sintering

3.2.1. Densification and conversion, temperature effect and dwell effect.

Table 2 shows the results of the sintering parameters evaluated. Both sintering temperature and sintering dwell were explored. Regarding the sintering temperature effect the porosity showed to be more illustrative for understanding the densification, clearly full density was achieved at treatments of 1300 °C or higher; while under-fired ceramics presented 37 and 15% of porosity (1100 °C and 1200 °C respectively). Density was rapidly increased with the increase of the maximum temperature up to 1300 °C, higher treatments resulted in a mild decrease, in the density value, probably not because of the formation of closed pores but to the phases evolution, since mullite has a lower density (3.71 g/cm^3) than alumina and zircon (4.0 and 4.6 g/cm^3 respectively). This was corroborated in the XRD analysis carried out in the following section. Fig. 5

Concerning the dwell time effect in the reaction sintering, at 1400 °C, the open porosity observed was below 0.3% for all the obtained samples, so they can be considered as dense composites. On the other hand, the density showed a similar behavior to the one observed for the temperature effect. The longer treatments presented an important decrease on the density, verifying that during the dwell some chemical processes occur.

Table 2
Density and porosity evolution as function of the sintering temperature and sintering time.

Sintering temperature (°C)	Time (min)	Density (g/cm^3)	Porosity (%)
SPS Temperature effect			
1100	10	2.64	38.19
1200	10	3.66	14.89
1300	10	4.36	0.01
1400	10	4.19	0.05
1500	10	3.84	0.0
Dwell time effect			
1400	10	4.19	0.05
1400	30	4.02	0.24
1400	60	3.87	0.1

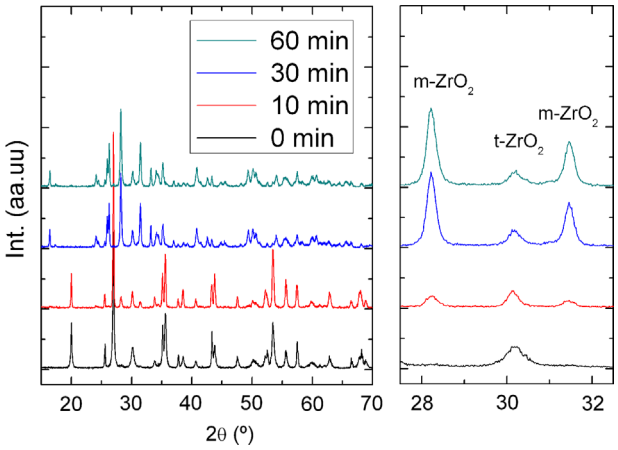

Fig. 5. Diffraction patterns of the ceramic composites sintered with different dwell time (at 1400 °C).

Fig. 6. SEM image of the Vickers indentation of the mullite–zirconia material sintered at 1500 °C with a 10 min soaking.

Fig. 6 shows the diffraction patterns of the different materials obtained after different sintering times. As expected, all the samples only presented the peaks corresponding to alumina, mullite, zircon and/or zirconia (m–ZrO_2 and t–ZrO_2). These phases were quantified by the Rietveld method [26,27]. Table 3 shows the final phase contents of the elaborated composites. The partial (almost 30%) zircon dissociation into crystalline zirconia and amorphous silica was also evidenced in these measurements. It can be observed clearly that the phase change is abrupt between 1400 and 1500 °C; after the 1400 °C treatment the reactions have not started and after 1500 °C the conversion is complete. This fact justifies the time study carried out for this temperature (1400 °C). In conclusion the mullitization temperature is at least 50 °C below of the un-milled mixtures employed in similar conditions by other authors [23]. Although mullite zirconia is obtained by reaction sintering in this processing route the densification occurs at 1300 °C and the reaction between 1400 and 1500 °C, these two processes are consecutive and not simultaneous.

Details of the diffraction patterns can also be observed in Fig. 6 as an inset in the top right corner. There the principal zirconia peaks (m–ZrO_2 (111), m–ZrO_2 (1-11) and t–ZrO_2 (101)) are shown. In the after-milled powder, the zirconia present in the 1100 °C treated sample is all tetragonal zirconia. After different sintering programs, up to 1400 °C, the amount of t–ZrO_2 decreases (linearly) and the amount of m–ZrO_2 increases, this is clearly observed from the values shown in Table 3. Only after the complete conversion (1500 °C) the monoclinic phase is the principal zirconia phase, evidencing that the product of the reaction is monoclinic and not tetragonal.

The m–ZrO_2 is stable at room temperature and the t–ZrO_2 is not stable at room temperature. It can be metastable if it is doped with different cations or if the grain size is smaller than a critical size [1,30,31]. In this study no cations were incorporated hence the presence of metastable t–ZrO_2 at room temperature on the developed composites is due to the small grain size of the produced zirconia.

Fig. 7 shows crystalline evolution during dwell time: again the crystalline phase detected were alumina, mullite, zircon and/or zirconia (m–ZrO_2 and t–ZrO_2). The inset detail permits to observe the evolution of the zirconia phases. The XRD-Rietveld Quantification results were shown in Table 3. The reaction is incipient after 10 min dwell and almost complete after 30 min and

Table 3
XRD—Rietveld quantification results.

Sample	Temp. (°C)	Dwell ($_{min}$)	Alumina	Zircon	Mullite	Zirconia			
			Al_2O_3	$ZrSiO_4$	$3Al_2O_3 \cdot 2SiO_2$	Total	m–ZrO_2	t–ZrO_2	t/m
SPS Temperature effect									
111	1100	10	47.9	41.5	2	8.6	0.8	7.8	9.75
121	1200	10	48	41.2	1.5	8.2	1.8	6.4	3.56
131	1300	10	51.3	38.7	0.5	9.8	3	6.8	2.27
141	1400	10	50.9	37.4	1.2	9.5	5.7	4.8	0.84
151	1500	10	–	–	56	44	41.2	2.8	0.07
Dwell time effect									
141	1400	10	50.9	37.4	1.2	9.5	5.7	4.8	0.84
143	1400	20	11.3	0.5	52	36.7	31.8	4.9	0.15
146	1400	20	13.4		49.5	37.1	32.8	4.3	0.13

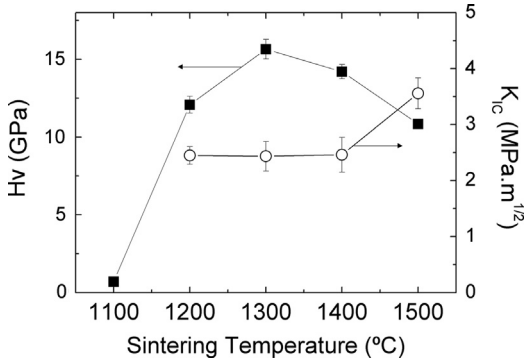

Fig. 7. Vickers Hardness (*Hv*) and fracture toughness (K_{IC}) of the sintered composites as a function of the sintering temperature (10 min dwell).

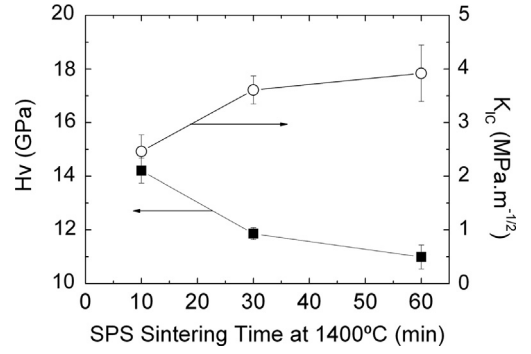

Fig. 8. Vickers Hardness (Hv) and fracture toughness (K_{IC}) of the sintered composites as a function of the dwell time.

60 min treatments. The presence of alumina in the long treated samples evidences that the reaction was incomplete even after 1 h treatments (long enough for SPS processing [3–5]). The absence of zircon might be explained by that fact that there might be some zircon like phase, with such low crystallinity that cannot be detected by XRD, this kind of zircon was detected in a similar system [32,33].

The m and t contents are shown in Table 3 as well; the conversion is incipient for the initial (10 min) treatments. The zirconia content is 10% and with the t/m proportion almost unitary and t–ZrO_2 is almost equal to the m–ZrO_2 content, for longer treatments the t–zirconia content remains constant while the m–ZrO_2 increases abruptly with the reaction. On the other hand t–ZrO_2 content remains constant (5 wt%) with maintenance time.

The sum of both zirconias is lower than the one achieved by the 1500 °C-10 min treatment. This is important because the zirconia reinforcement mechanisms depend on the amount, type and size of the zirconia grains imbibed in the ceramic matrix.

3.2.2. *Mechanical properties (Hv and K_{IC})*

Toughening enhancement can be obtained by incorporating zirconia particles (ZrO_2) in a ceramic matrix. Several concurrent mechanisms are involved in the toughening: stress-induced transformation, micro-cracking, crack bowing and crack deflection and also the thermal expansion mismatch. However, as the content of tetragonal zirconia is nearly

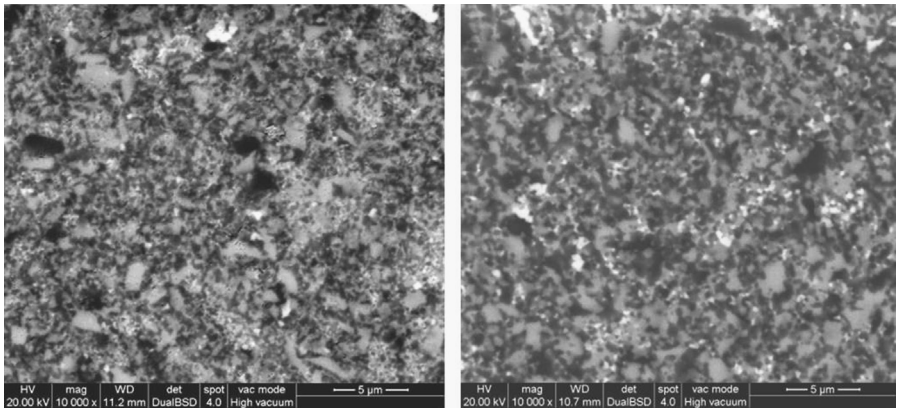

Fig. 9. SEM image of the composites sintered at 1300 °C and 1400 °C, with 10 min soaking. (For interpretation of the references to color in this figure, the reader is referred to the web version of this article.)

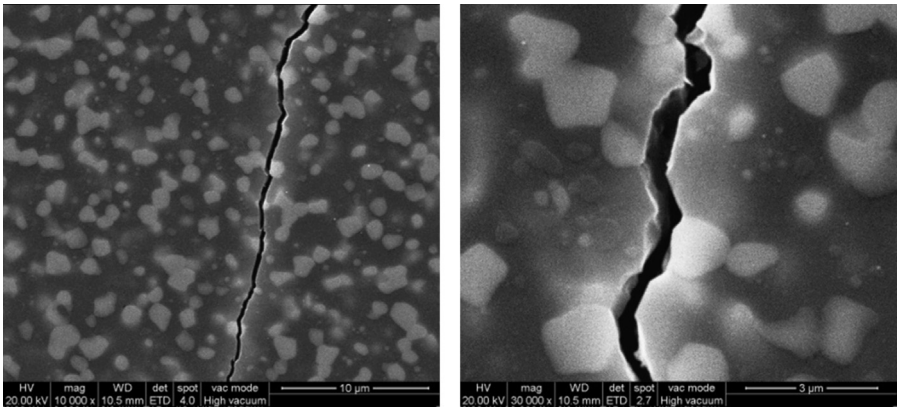

Fig. 10. Intergranular cracks through the mullite matrix of the fully densified and fully converted mullite–zirconia composite material (SEM Images *x*10,000 and 30,000).

Table 4
Comparison of materials' mechanical properties with the data reported in literature.

[Ref]	Processing route	Density (%)	*Hv* (GPa)	K_{IC} (MPa $m^{1/2}$)	Flexural strength σ_f (MPa)	E (GPa)
[11]	Slip casting, pressureless sintering. 1400–1600 °C	≈ 92	9–12	2.2–3.9		
[12]	Isostatic pressing pressureless sintering. 1400–1600 °C	≥ 99	5.6 8.2	3.7 5.0	160 330	
[13]	Isostatic pressing 1600 °C	≈ 98		4.2	215	150
[14]	Isostatic pressing, pressureless sintering 1570 °C 1670 °C	≈ 99		2.1–3.2		
[15]	Plasma fused 50 kW thermal plasma reactor was used for plasma fused and plasma sintering techniques	≈ 98	10–14			
[16]	Direct sintering of mullite–zirconia grains and zircon obtained from slip casting	≈ 95			100–170	145–170
[17]	Direct sintering of Mullite–zirconia grains and zircon obtaines from slip casting	≈ 95		1.75–3.0	100–170	140–225
[18]	In-situ controlled crystallizing from SiO_2–Al2O_3–ZrO_2 amorphous bulk	≈ 99	13.72	5.13	520	
[19]	Coastal sillimanite beach sand, alumina and zirconia powder were used as the main raw materials for uniaxial pressing and pressureless sintering 1650 °C	≈ 99	4.8–5.8	2.7–3.6		130–198
[20]	Spark plasma reaction sintering of ZrO_2–mullite composites from plasma spheroidized zircon/alumina powders	99	6–13	3–11		130–300
[21]	Isostatic pressing pressureless sintering. 1400–1650 °C; Y2O3 addition ≤ 7%	≈ 99	5.5–10	2.4–5.2	142–255	
This study	HEM + SPS	≥ 99.5	10–15	2–4		

negligible, the transformation toughening mechanism should be discarded as first approach.

Fig. 8 shows the Vickers indent in the polished surface of the totally converted dense ceramic, the homogeneous microstructure is easily observed. The relation between the indent size and the microstructure are adequate to apply the indentation method [28].

The hardness (*Hv*) and fracture toughness (K_{IC}) are plotted as a function of the sintering temperature in Fig. 9. The observed behavior was different. While *Hv* abruptly increased up to 1500 MPa with the sintering temperature below 1300 °C, temperature where fully densification was achieved. After this, *Hv* decreased with the sintering temperature, the values are comparable with the ones obtained by different processing routes. This might be related the reaction evolution. On the other side K_{IC} remained constant (≈ 2.5 MPa $m^{1/2}$) between 1200 °C and 1400 °C not depending on the reaction sintering evolution. On the other hand the toughness value of the composite processed at 1500 °C presented value over 3.5 MPa $m^{1/2}$. This fact represents a remarkable increase near to 40% in K_{IC}.

The hardness (*Hv*) and fracture toughness (K_{IC}) are plotted as a function of the dwell time: the behavior is consistent with the first experiment (plotted in Fig. 10). Again the obtained values for *Hv* and K_{IC} are comparable with the literature values. Remembering that the densification was already achieved, it can be concluded that the hardness decreases with the reaction evolution and that the toughness is increased with the conversion. The achieved K_{IC} are comparable with the ones obtained by different processing routes.

In Table 4 the materials obtained are compared with the data reported in literature for dense mullite zirconia materials obtained by different processing routes. From this it can be clearly observed that the results obtained by this processing route are comparable. And the properties are sometimes better than the ones obtained by traditional routes like slip casting, uniaxial pressing and pressure-less sintering. The advantage of the high energy milling is also observed.

3.2.3. Microstructural analysis

Fig. 9 shows that the typical microstructure of the un-reacted alumina zircon dense ceramic (materials processed between

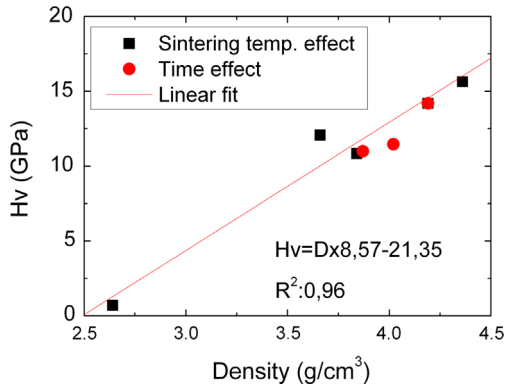

Fig. 11. Linear correlation between Hardness (*Hv*) and density in the studied composites.

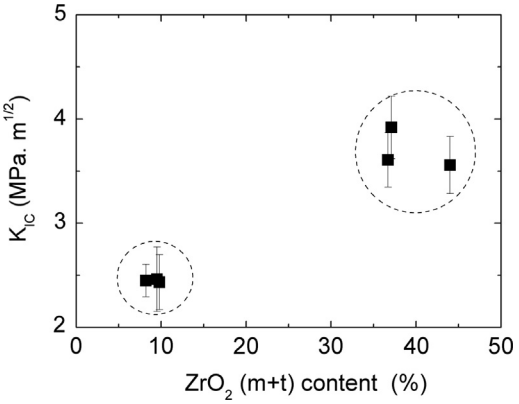

Fig. 12. Fracture toughness (K_{IC}) of the sintered composites as a function of the zirconia content evaluated by the Rietveld method. (For interpretation of the references to color in this figure, the reader is referred to the web version of this article.)

1300 and 1400 °C) presented this microstructure. The material is almost fully densified (concordant with Archimedes results), only some close micro-pores can be observed in dark. The grain growth was minimized by the short holding time and by the rapid heating rate. The microstructure consists in zircon (middle gray) grains (2–4 μm size) imbibed in a finer matrix of un-reacted alumina grains. Small amount of minor (≤ 1 μm) zirconia grains (white), detected by XRD in the milled powder, can be observed in some zircon grain boundaries.

As in previous works [9–10], the high pressure (100 MPa) and the elevated temperatures (1300 °C) together with the electrical current of the SPS processes are suitable conditions to achieve the near full densification of the milled powders. The shape and size of the zircon grains did not change significantly after the sintering.

A detail of the resulting microstructure can be observed in the following figures (Fig. 12). These show the microstructure together with the crack developed in the Vickers test. The tortuous crack typical path can be observed.

For the completely converted materials (sintered at 1500 °C) the microstructure is a well-defined mullite (dark) ceramic matrix with a homogeneous distribution of imbibed zirconia grains (light gray), this microstructure is comparable to the one obtained by different processing routes [2] [11–22]. The zirconia grain size is between 2–5 μm. These are similar to the starting zircon grains. The zirconia grains gave planar borders and rounded corners. The crack is intra-granular for the zirconia grains and inter-granular for the mullite matrix. This may explain the increase in the K_{IC}.

The concurrent effects the powder mechanical activation and the current activation sintering process may explain the lower sintering temperature in comparison with the hot pressing or pressureless sintering. Even below the temperature achieved by SPS sintering of un-milled powders. The wanted interlocking configuration (Fig. 10) achieved enhanced the mechanical properties of these materials observed in the previous section.

The microstructure evolution with the temperature dwell in the densified and un-reacted material (sintered at 1400 °C) was

also studied but SEM images are not shown in order to keep the article size adequate. The incipient reaction (10 min dwell) was previously observed in Table 3. The other two (30 and 60 min) were concordant to the quantification performed by XRD. No important amount of zircon grains can be observed, mullite and zirconia were the principal phases. In all the cases mullite acts as a continuous matrix and the rounded zirconia (2–5 μm) grains are imbibed in this matrix, furthermore some zirconia grains are not completely isolated, but the microstructure configuration is not percolated. The 60 min sintered material presents a completed conversion while the intermediate material presents some un-reacted zircon grains.

3.3. Vickers hardness–density correlation

Fig. 11 shows the Vickers Hardness value of all the studied composites as a function of the density evaluated by the Arquimedes method. The result of the linear fit is shown as well. Showing that for this family of materials *Hv* is strongly related with the density. And not associated to the densification (porosity).

3.4. Zirconia toughening

Significant toughening can be obtained by incorporating zirconia particles (ZrO_2) in a ceramic matrix. Different mechanisms are involved in the toughening: stress-induced transformation, micro-cracking, crack bowing and crack deflection. In all cases, the operative toughening mechanism depends on such variables as matrix stiffness, zirconia particle size, chemical composition, temperature and strength [18] [1,30,31]. For that K_{IC} is plotted against the amount of total ZrO_2 (estimated by the Rietveld method) in Fig. 12. As mentioned this Zirconia was formed from the zircon dissociation (t–during the mechanical pre-treatment and m–ZrO_2 during the SPS treatment. Although six different materials with different processing conditions, varying, the maximum temperature and dwell time were studied there are clearly two situations in terms of the relation between K_{IC} and the amount of ZrO_2 clearly shown in Fig. 12. While the incomplete conversion materials (ZrO_2 $\approx$ 10 wt%) presented a K_{IC} of $\approx$ 2.5 MPa $m^{1/2}$, the materials where the conversion, from alumina and zircon to mullite and zirconia, is complete (or almost complete) with high Zirconia content ($\geq$ 35wt%) presented a higher K_{IC} between 3.4 and 4.0 MPa $m^{1/2}$. Showing that for dense materials, the resulting crystalline phase and microstructural configuration of a ceramic matrix (mullite or mullite–alumina) result in a material with a considerably higher toughness.

4. Conclusions

A series of ceramic dense composites from the Al_2O_3–SiO_2–ZrO_2 system were elaborated, the employed processing route consisted in the SPS sintering of high energy milled zircon alumina stoichiometric mixtures of fine grained (0.5–5 μm) commercial powders.

The employed mechanical pretreatment resulted in a homogeneous dry mixture with a partial ($\approx$ 20%) zircon dissociation, apparently enhanced by the alumina presence. This together with the posterior SPS processing permitted to obtain fully dense ceramic composites at a very low temperature (1300 °C) with no additive required. The reaction from alumina zircon mixtures to mullite zirconia occur 200 °C below conventional processing routes and at least 50 °C below the reported SPS based materials processed from un-milled mixtures. The microstructure and mechanical properties obtained were comparable to the ones obtained by other processing routes. Finally interesting correlations were found for the developed materials group: while the hardness is directly correlated to the material density and independent to the conversion, the fracture toughness is correlated to the zirconia (m+t) content within the range of dense composites studied.

Summary of novel conclusions

HEM followed by SPS permitted to obtain dense mullite zirconia ceramics by reaction-sintering at low temperatures without the requirement of any additive. Hardness and toughness correlate with density and conversion.

References

[1] N. Claussen, J. Jahn, Mechanical properties of sintered, in situ-reacted mullite–zirconia composites, Journal of the American Ceramic Society 63 (3–4) (1980) 228–229.
[2] H.H. Zender, H. Leistner, H.R. Searle, ZrO_2 materials for application in the ceramic industry, Interceram 39 (6) (1990) 33–36.
[3] M. Omori, Sintering, consolidation, reaction and crystal growth by the spark plasma system (SPS), Materials Science and Engineering A 287 (2) (2000) 183–188.
[4] R. Orru, R. Licheri, A.M. Locci, A. Cincotti, G. Cao, Consolidation/synthesis of materials by electric current activated/assisted sintering, Materials Science and Engineering R: Reports 63 (4–6) (2009) 127–287.
[5] S. Grasso, Y. Sakka, G. Maizza, Electric Current Activated/Assisted Sintering (ECAS): a review of patents 1906–2008, Science and Technolgy of Advanced Materials 10 (2009) 053001.
[6] C. Suryanarayana, Mechanical alloying and milling, Progress in Materials Science 46 (1–2) (2001) 1–184.
[7] G.-D. Zhan, J. Kuntz, J. Wan, J. Garay, A.K. Mukherjee, A novel processing route to develop a dense nanocrystalline alumina matrix (< 100 nm) nanocomposite material, Journal of the American Ceramic Society 86 (1) (2003) 200–202.
[8] K. Morita, K. Hiraga, B.-N. Kim, H. Yoshida, Y. Sakka, Synthesis of dense nanocrystalline ZrO_2–$MgAl_2O_4$ spinel composite, Scripta Materialia 53 (9) (2005) 1007–1012.
[9] N.M. Rendtorff, S. Grasso, C. Hu, G. Suarez, E.F. Aglietti, Y. Sakka, Dense zircon ($ZrSiO_4$) ceramics by high energy ball milling and spark plasma sintering, Ceramics International 38 (3) (2012) 1793–1799.
[10] N.M. Rendtorff, S. Grasso, C. Hu, G. Suarez, E.F. Aglietti, Y. Sakka, Zircon–zirconia ($ZrSiO_4$–ZrO_2) dense ceramic composites by spark plasma sintering, Journal of the European Ceramic Society 32 (4) (2012) 787–793.
[11] L.B. Garrido, E.F. Aglietti, L. Martorello, M.A. Camerucci, A.L. Cavalieri, Hardness and fracture toughness of mullite–zirconia composites obtained by slip casting, Materials Science and Engineering: A 419 (1–2) (2006) 290–296.
[12] Kaberi Das, G. Banerjee, Mechanical properties and microstructures of reaction sintered mullite–zirconia composites in the presence of an

additive—dysprosia, Journal of the European Ceramic Society 20 (2) (2000) 153–157.
[13] T. Koyama, S. Hayashi, A. Yasumori, K. Okada, M. Schmucker, H. Schneider, Microstructure and mechanical properties of mullite–zirconia composites prepared from alumina and zircon under various firing conditions, Journal of the European Ceramic Society 16 (2) (1996) 231–237.
[14] M. Hamidouche, N. Bouaouadja, H. Osmani, R. Torrecillias, G. Fantozzi, Thermomechanical behaviour of mullite–zirconia composite, Journal of the European Ceramic Society 16 (1996) 441–445.
[15] J.S. Moya, M.I. Osendi, Microstructure and mechanical properties of mullite/ZrO_2 composites, Journal of Materials Science 19 (1984) 2909–2914.
[16] Sasmita Prusty, D.K. Mishra, B.K. Mohapatra, S.K. Singh, Effect of MgO in the microstructure formation of zirconia mullite composites from sillimanite and zircon, Ceramics International 38 (3) (2012) 2363–2368.
[17] N. Rendtorff, L. Garrido, E. Aglietti, Mullite–zirconia–zircon composites: properties and thermal shock resistance, Ceramics International 35 (2) (2009) 779–786.
[18] N.M. Rendtorff, L.B. Garrido, E.F. Aglietti, Zirconia toughening of mullite–zirconia–zircon composites obtained by direct sintering, Ceramics International 36 (2) (2010) 781–788.
[19] S.-Q. Liang, X.-P. Tan, S.-Q. Li, Y. Tang, Structure and mechanical properties of ZrO_2–mullite nano-ceramics in SiO_2–Al_2O_3–ZrO_2 system, Journal of Central South University of Technology (English Edition) 14 (1) (2007) 1–6.
[20] Manas Kamal Haldar, Effect of magnesia additions on the properties of zirconia–mullite composites derived from sillimanite beach sand, Ceramics International 29 (5) (2003) 573–581.
[21] K.A. Khor, L.G. Yu, Y. Li, Z.L. Dong, Z.A. Munir, Spark plasma reaction sintering of ZrO2–mullite composites from plasma spheroidized zircon/alumina powders, Materials Science and Engineering: A 339 (1–2) (2003) 286–296.
[22] Kaberi Das, B. Mukherjee, G. Banerjee, Effect of yttria on mechanical and microstructural properties of reaction sintered mullite–zirconia composites, Journal of the European Ceramic Society 18 (12) (1998) 1771–1777.
[23] M.C. Anjali, P. Biswas, D. Chakravarty, U.S. Hareesh, Y.S. Rao, R. Johnson, Low temperature in-situ reaction sintering of zircon:alumina composites trough spark plasma sintering, Science of Sintering 44 (3) (2012) 323–330.
[24] E. Rocha-Rangel, S. Díaz-de-la-Torre, M. Umemoto, H. Miyamoto, H. Balmori-Ramírez, Zirconia–mullite composites consolidated by spark plasma reaction sintering from zircon and alumina, Journal of the American Ceramic Society 88 (5) (2005) 1150–1157.
[25] A.V. Hmelov, I. Shteins, Properties of mullite–zirconium ceramic obtained by spark plasma sintering, Glass and Ceramics (English translation of Steklo i Keramika) 68 (11–12) (2012) 399–404.
[26] D.L. Bish, J.E. Post, Quantitative mineralogical analysis using the Rietveld full-pattern fitting method, American Mineralogist 78 (9–10) (1993) 932–940.
[27] H.M. Rietveld, A profile refinement method for nuclear and magnetic structures, Journal of Applied Crystallography 2 (1969) 65–71.
[28] Koichi Niihara, New design concept of structural ceramics. Ceramic nanocomposites, Nippon Seramikkusu Kyokai Gakujutsu Ronbunshi/Journal of the Ceramic Society of Japan 99 (1154) (1991) 974–982.
[29] A. Kaiser, M. Lobert, R. Telle, Thermal stability of zircon ($ZrSiO_4$), Journal of the European Ceramic Society 28 (11) (2008) 2199–2211.
[30] P.M. Kelly, L.R.F. Rose, The martensitic transformation in ceramics—Its role in transformation toughening, Progress in Materials Science 47 (5) (2002) 463–557.
[31] X.-J. Jin, Martensitic transformation in zirconia containing ceramics and its applications, Current Opinion in Solid State and Materials Science 9 (6) (2005) 313–318.
[32] N.M. Rendtorff, M.S. Conconi, E.F. Aglietti, C.Y. Chain, A.F. Pasquevich, P.C. Rivas, J.A. Martínez, M.C. Caracoche, A short and long range study of mullite–zirconia–zircon composites, Hyperfine Interactions 198 (1) (2010) 219–228.
[33] N.M. Rendtorff, M.S. Conconi, E.F. Aglietti, C.Y. Chain, A.F. Pasquevich, P.C. Rivas, J.A. Martínez, M.C. Caracoche, Phase quantification of mullite–zirconia and zircon commercial powders using PAC and XRD techniques, Hyperfine Interactions 198 (1) (2010) 211–218.